Int. J. Electrochem. Sci., 17 **(2022)** Article Number: 220218, doi: 10.20964/2022.02.18

International Journal of
ELECTROCHEMICAL
SCIENCE
www.electrochemsci.org

A Variable-length scale Parameter Dependent State of Charge Estimation of Lithium Ion Batteries by Kalman Filters

Minkyu Kwak[1], *Bataa Lkhagvasuren*[1,*], *Hong Sung Jin*[1], *Gyuwon Seo*[2], *Sungyool Bong*[2,3], *Jaeyoung Lee*[2,3]

[1] Department of mathematics, Chonnam National University, Gwangju, Republic of Korea
[2] School of Earth Science and Environmental Engineering, Gwangju Institute of Science and Technology (GIST), Gwangju, Republic of Korea
[3] ERTL Center for Electrochemistry and Catalyst, Gwangju Institute of Science and Technology (GIST), Gwangju, Republic of Korea
[*]E-mail: bataa@chonnam.ac.kr

Received: 4 October 2021 / *Accepted:* 29 November 2021 / *Published:* 5 January 2022

This paper proposes a new state of charge (SOC) estimation algorithm based on Kalman filters (KF). In the first stage, the equivalent circuit model's parameters are estimated by a least square estimation window-wise, assuming a linear SOC and open-circuit voltage (OCV) relation. The algorithm accurately estimates the parameters and observes the changes that depend on SOC. Moreover, based on the estimated parameters, the OCV values are identified. In the next stage, window-wise Kalman filter(ES-KF) without hysteresis voltage and extended Kalman filter (ES-EKF) and sigma-point Kalman filter (ES-SPKF) algorithm with hysteresis voltage are executed to estimate SOC. Having fewer state equations and hysteresis parameters tuned up, the ES-EKF and ES-SPKF perform accurately and improve the results of previous algorithms. The proposed methods are validated by experiments with three different datasets obtained from lab tests. We also show SOC-OCV curve can be obtained in a simple way that replaces the time-consuming C/30 tests.

Keywords: Parameter estimation, State of charge, Battery, Kalman filter, Battery management system

1. INTRODUCTION

The battery is the most attractive energy storage device, because of its high energy density and portability. Portable utilities, electric vehicles, and industries use batteries as their main energy storage device. Various battery technologies are being developed and the energy and power densities of the batteries are continuously advancing. Nowadays, lithium-ion batteries are being used extensively for their higher energy density, longer cycle life, and more environmental friendliness.

Electric vehicles (EV), and Plug-in hybrid-electric vehicles (PHEV) are recent technologies to achieve efficient utilization of energy sources. To ensure safety and efficiency, the battery management system (BMS) monitors and controls the battery states and operations by measuring the current, voltage, and temperature. The SOC, which is the level of the remaining charge relative to the total capacity, is a crucial parameter and is among the states that need to be monitored. Estimating SOC is the fundamental challenge for BMS because the parameter uncertainty and nonlinear dynamics of the battery make it a complex and difficult task.

Broadly, the SOC estimation methods can be divided into two categories; model-free methods and model-based methods. Ampere-hour counting (Ah counting) [1] is the most basic model-free method to estimate SOC. In this method, SOC is calculated by integrating the loaded current to determine how much charge is remained. Although, Ah counting is a useful theoretical method, it can not be used in a practice, because it suffers from the unknown initial SOC value and the accumulated uncertainty due to the integration process. Therefore, a proper recalibration must be incorporated into it and Ah counting method is often combined with other techniques to obtain better accuracy. Another conventional model-free method is using look-up tables or SOC-OCV relation. This approach is used independently or in a combination of Ah counting [2, 3]. However, measuring OCV requires a long rest time, therefore, it is not used in online applications. Another class of model-free methods are data-driven methods. Data-driven methods [4, 5, 6, 7] use various techniques such as neural networks, support vector machines and fuzzy logic to train black-box battery model based on the empirical data for the purpose of SOC estimation. The advantage of these methods is they do not require deep domain-specific knowledge of the batteries [8]. However, they may need a large amount of training data and preparatory work to achieve an accuracy.

More sophisticated approaches are the model-based SOC estimation methods [9]. Basically, there are two types of battery models: electrochemical and electrical models. The electrochemical models use equations based on physical laws that govern the internal electrochemical processes in the battery. Although the electrochemical models are very accurate, the coupled partial differential equations make them very difficult to implement. An electrical model uses electrical circuit elements such as voltage source, resistors, and capacitors, to describe battery dynamic behavior. It is ideal for system simulation and implementation in embedded microcontrollers [10-12]. From the view of SOC estimation, based on the battery modeling, the current literature consists of two types estimation methods: sequential probabilistic inference methods and observer-based techniques. With the assumption of Gaussian noises, Kalman filter (KF) and its variants such as extended KF (EKF), sigma-point KF (SPKF), and cubature KF are Gaussian sequential probabilistic inference methods and they have been successfully applied to the SOC estimation problems [13-22]. The EKF is a widely used nonlinear KF and it linearizes the system dynamics efficiently. In the works [15, 23], the authors employed EKF with the electrical model for SOC estimation. If the noise covariance matrices initialized properly and the model parameters are tuned up, the KF based methods perform accurately and continuously. The unscented KF and central difference KF methods [14, 24, 25, 26, 19], which are different forms of SPKF, address model nonlinearities more efficiently. Extensive and exhaustive experimental tests considering different forms of nonlinear KFs and parameter identifications (with or without hysteresis model) were presented in [19].

Particle filter (PF) is another type of sequential probabilistic inference scheme that deals with non Gaussian noise. PFs approximate the probability density functions of nonlinear systems being modeled by Monte-Carlo simulations. Although, PFs give accurate results when the system nonlinearity is high, they require great computational resources [27, 28]. On the other hand, observer-based SOC estimations techniques are computationally efficient, since they employee the deterministic assumption. The literature includes various type of observer-based SOC estimation techniques: Luenberger observer [29-31], proportional integral observer [32], adaptive observer and sliding mode observer [33-36]. For the details of above-mentioned methods and the other ones such as reduced-order models, we refer to excellent review papers [37, 9, 38, 39, 40] and references therein.

The model parameters depend on the SOC, ambient temperature, and the age. Therefore, online parameter estimation algorithms are desirable for capturing SOC dependent change. In the works [41, 42, 31, 43, 36, 44], a sliding window least-square estimator was used. This method extracts the model parameters online taking into account the parameter changes during the battery operation and it has a better stability. However, this method uses look-up table to extract some parameters of piecewise linear model for SOC co-estimation. More efficient parameter estimation scheme, and least square SOC estimator were proposed in [45].

In this paper, we consider the natural extension of the parameter estimation scheme proposed in [45] and obtain more accurate, computationally efficient SOC estimator by KFs. The novelty of this paper is summarised as follows:

- We introduce a refined version of the discretization used in [45] to execute KF-family SOC estimation algorithms.
- The special discretization proposed in this paper allows to compute OCV values accurately window-wise, and therefore, the number of state equations in KF-family algorithms reduced by one and it saves the computational cost.
- The KF-family based co-estimation scheme, in which the OCV values are computed window-wise and the parameter variability is taken into account, yields more accurate results compared to the previously studied methods given in [13, 45].
- Our method allows to acquire SOC-OCV curve from the computed OCV values without C/30 tests.
- The proposed KF-family SOC estimation algorithm is a probabilistic method based on the electrical model. Therefore, the complicated electrochemical processes inside the battery are represented efficiently and the uncertainty is handled in an optimal way.

The rest of this article is organized as follows. The section 2 introduces the battery model, the proposed discretization, parameter identification scheme and discusses the use of KFs with and without the hysteresis effect for the identified parameters. In section 3, the experimental results with data obtained from lab tests were given to validate the proposed method.

2. BATTERY MODEL

In this work, we assume the terminal voltage V and current I are known only, and we do not consider the temperature dependence and the battery capacity degradation. An electrical model (or

equivalent circuit model) of a battery consists of a series resistance R_0 and parallel RC components (Fig.1). The purpose of using an electrical model is to imitate or approximate the dynamic behavior of a battery by the dynamics of the electrical model. Theoretically, one can add as many RC components as one wants. However, adding RC components increases the order of the dynamical systems (order of differential equations) being modeled. Although higher-order electrical models can give accurate simulation results, computational complexity and numerical stability issues often degrade the estimation results. In the work [10], two RC components are used to simulate the behavior of the Li-Po cells with reasonable accuracy. And each of the RC components acts as a slow and fast change of the variable. But one RC component model can yield good enough accuracy [31, 43, 15] for a shorter time window expressing faster transients.

The relation of OCV and SOC is nonlinear and contributes to the complexity of battery dynamics significantly. An approximation of the SOC-OCV curve by simpler functions (linear, quadratic, sigmoid, etc.) is necessary to manipulate the model's underlying equations. In this paper, one RC component model is considered as in the Fig.1, and the SOC-OCV curve is represented by:

$$\mathrm{OCV} = \mathrm{f(SOC)}. \tag{1}$$

The terminal voltage V is the sum of individual element voltages:

$$\mathrm{V} = \mathrm{OCV} + \mathrm{V_0} + \mathrm{V_{RC}}, \tag{2}$$

where V_0 is the voltage across the resistor element R_0 and V_{RC} is the voltage across the RC component. The V_{RC} follows the differential equation

$$\dot{\mathrm{V}}_{\mathrm{RC}} = -\frac{1}{\mathrm{RC}}\mathrm{V_{RC}} + \frac{1}{\mathrm{C}}\mathrm{I}. \tag{3}$$

Combining (2) and (3) yields

$$\mathrm{RC\dot{V}} - \mathrm{RCR_0\dot{I}} - (\mathrm{R_0} + \mathrm{R})\mathrm{I} + \mathrm{V} = \mathrm{OCV} + \mathrm{RCO\dot{C}V}. \tag{4}$$

The SOC, by definition, satisfies the equation

$$\mathrm{S\dot{O}C} = \frac{\eta}{\mathrm{Q}}\mathrm{I}, \tag{5}$$

where Q is the total capacity of the cell and η is the Coulombic efficiency. For the time window $\{t_k\}$, $k = k_0, k_0 + 1, \ldots, k_0 + n$, we approximate the SOC-OCV curve by linear relation

$$\mathrm{OCV} = \mathrm{aSOC} + \mathrm{b}, \tag{6}$$

where a and b are constants. This approximation is reasonable one if the time window and range of variability for SOC are short.

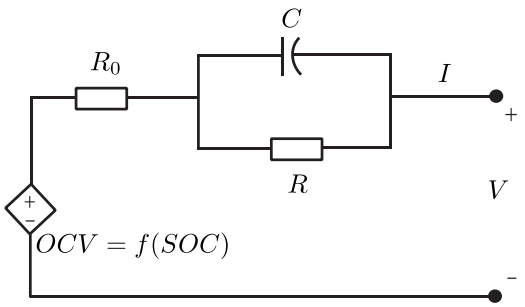

Figure 1. Battery circuit model with one RC branch

Putting (6) into (4) gives

$$RC\dot{V} - RCR_0\dot{I} - \left(R_0 + R + \frac{aRC\eta}{Q}\right)I + V = aSOC + b. \tag{7}$$

2.1. Parameter identification

Since the equations (7) are an overdetermined system of linear equations, a simple linear least square method can be invoked to extract the parameters. In order to discretize the equations (7), we use the trapezoidal rule as follows:

$$\begin{aligned} f\big((k+1/2)T\big) &= \tfrac{f[k+1]+f[k]}{2}, \\ \dot{f}\big((k+1/2)T\big) &= \tfrac{f[k+1]-f[k]}{T} \end{aligned} \tag{8}$$

where $f[k] = f(kT)$. The bilinear transform, which is a transformation from continuous time system (in the Laplace domain) to discrete time system (in the Z-domain) uses the trapezoidal rule (8). Unlike the method used in [31], where the bilinear transform is applied to the second order version of (8) (one more differentiation), the trapezoidal rule is applied to (7) directly. In the next stage, the SOC is expressed by coulomb counting method with the rectangle rule for integral:

$$SOC[k] = SOC[k_0] + \frac{T\eta}{Q}(J[k] - I[k]) \tag{9}$$

with $J[k] = \sum_{j=k_0}^{k} I[j]$ for $k = k_0, k_0 + 1, \ldots, k_0 + n$.

In the work [45], trapezoidal rule for integral was used for coulomb counting. The reason that we use the rectangle rule for integral in this paper is the equation (9) is compatible with the state equation in KF-based SOC estimation.

Using (8) for V, I and computing SOC by (9), we obtain the following discrete differential equations:

$$V[k+1] = a_1V[k] + a_2I[k+1] + a_3I[k] + a_4J[k] + a_5 \tag{10}$$

where

$$\begin{aligned} a_1 &= \frac{2RC - T}{2RC + T}, \\ a_2 &= \frac{2RCR_0 + T(R_0 + R + aRC\eta/Q)}{2RC + T}, \\ a_3 &= \frac{-2RCR_0 + T(R_0 + R + aRC\eta/Q) - aT^2\eta/Q}{2RC + T}, \\ a_4 &= \frac{2aT^2\eta}{Q(2RC + T)}, \\ a_5 &= \frac{2TOCV[k_0]}{2RC + T}. \end{aligned} \tag{11}$$

The values $V[k+1], V[k], I[k+1], I[k], J[k]$ are known (measured) values within the current time window, the system (10) and (11) can be solved in a least square sense. Therefore, the parameters a, R_0, R, C and the value $OCV[k_0]$ are estimated directly. The least square estimation needs a proper variability in the inputs in order to yield a stable solution. Less variability causes numerical instability and too much variability yields a longer time window length, which is undesirable from the view of

online estimations. In this work, the variability of inputs expressed by the excitation level. The excitation level measured by the jumps of the current input and is counted as one if

$$|\mathrm{I}[\mathrm{k}+1]-\mathrm{I}[\mathrm{k}]|>\frac{\mathrm{Q}}{\mathrm{e}} \tag{12}$$

satisfies. Here, e is a constant to tolerate some noise and the value $\mathrm{e}=1000$ is used in this work. If the excitation level reaches a certain threshold, the length of the time window is determined. This simple scheme feeds variable-length time windows into the least square estimator.

In general, there are two types of implementations of the least square algorithms; the block (BLS) and recursive (RLS) forms. In the BLS estimation, all the measurement variables are collected at once and a least square problem is solved for the whole data. The main disadvantage of the BLS algorithm is its computational cost, when it is applied to the sequential data processing problem. When a new measurement becomes available, the whole estimation needs to be repeated. The RLS estimation is computationally efficient as it aggregates the current measurement to the previous computation. However, the RLS estimation depends on the initial value and it suffers from the convergence problem and the loss of parameter tracking. Its improved version, forgetting parameter RLS, is often used in battery parameter estimation [20, 46, 47]. Note that there is no mechanism to choose the time window size in RLS applications of battery parameters, as the RLS estimation runs continuously. Moreover, the least square estimator should stop when there is not enough information about the dynamics (excitation). However, our implementation of the excitation level in the battery parameter estimation makes BLS algorithm a perfect choice. As soon as the window size is determined based on the excitation level, the BLS is executed once for only that time window and there is no redundant computation. This parameter estimation strategy eliminates both problems of BLS and RLS algorithms at the same time. We refer to [48] for detailed discussions of variable-length least square parameter estimation.

In the next stage, if we are to ignore the hysteresis effect, the value $\mathrm{SOC}[\mathrm{k}_0]$ and the parameter b can be determined by

$$\mathrm{SOC}[\mathrm{k}_0]=\mathrm{f}^{-1}(\mathrm{OCV}[\mathrm{k}_0]),\ \mathrm{b}=\mathrm{OCV}[\mathrm{k}_0]-\mathrm{aSOC}[\mathrm{k}_0]. \tag{13}$$

The estimation algorithm purposed in [31] was able to determine only 4 parameters $\mathrm{a}, \mathrm{R}_0, \mathrm{R}, \mathrm{C}$ in the first stage and a look-up table of piece-wise linearization of SOC-OCV curve was used to determine b. However, the estimation scheme (10)-(13) determines not only the parameters $\mathrm{a}, \mathrm{b}, \mathrm{R}_0, \mathrm{R}, \mathrm{C}$, but also the initial values of $\mathrm{SOC}[\mathrm{k}_0]$ and $\mathrm{OCV}[\mathrm{k}_0]$. Moreover, the linearization (6) of SOC-OCV curve was performed within the time window, while the linearization purposed in was done statically (not depending on time). Therefore, our estimation scheme has a better adaptation, and extensive numerical testing results are reported in [45] for the original version. Since the initial value $\mathrm{OCV}[\mathrm{k}_0]$ was determined, the circuit voltage V_{RC} can be computed by

$$V_{RC}[k+1]=e^{-\frac{T}{RC}}V_{RC}[k]-R\left(e^{-\frac{T}{RC}}-1\right)I[k], \tag{14}$$

$$V_{RC}[k_0]=V[k_0]-OCV[k_0]-R_0I[k_0] \tag{15}$$

within time window. Consequently, the $OCV[k]$ values are determined by

$$OCV[k]=V[k]-V_{RC}[k]-R_0I[k]. \tag{16}$$

In the next section, we present the KF-based SOC estimation algoritm that use the values (16).

2.2. SOC *estimation by KFs*

Gaussian sequential probabilistic inference scheme is used for the following general model:

$$x_{k+1} = f(x_k, u_k, w_k), \quad (17a)$$

$$y_k = g(x_k, u_k, v_k) \quad (17b)$$

where w_k and v_k Gaussian noise processes with means $\bar{w}$ and $\bar{v}$ and covariance matrices Σ_w and Σ_v respectively. The following is the summary of general Gaussian sequential probabilistic inference scheme, where Plett's notations were used from [14].

Definition	
$\tilde{x}_k^- = x_k - \hat{x}_k^-$,	$\tilde{y}_k = y_k - \hat{y}_k$
$\Sigma_{\tilde{y},k} = E[(\tilde{y}_k)(\tilde{y}_k)^T]$	$\Sigma_{\tilde{x}\tilde{y},k}^- = E[(\tilde{x}_k^-)(\tilde{y}_k)^T]$
$Y_k = \{y_0, y_1, \dots, y_k\}$	
Initialization	
For $k = 0$, set	$\hat{x}_0^+ = E[x_0]$
	$\Sigma_{\tilde{x},0}^+ = E[(x_0 - \hat{x}_0^+)(x_0 - \hat{x}_0^+)^t]$
Predict	
State estimate	$\hat{x}_k^- = E[f(x_{k-1}, u_{k-1}, w_{k-1})\|Y_{k-1}]$
Covariance	$\Sigma_{\tilde{x},k}^- = E[(\tilde{x}_k^-)(\tilde{x}_k^-)^T]$
Update	
Output estimate	$\hat{y}_k = E[g(x_k, u_k, v_k)\|Y_{k-1}]$
Optimal Kalman gain	$L_k = \Sigma_{\tilde{x}\tilde{y},k}^- \Sigma_{\tilde{y},k}^{-1}$
State estimation	$\hat{x}_k^+ = \hat{x}_k^- + L_k[y_k - \hat{y}_k]$
Error covariance	$\Sigma_{\tilde{x},k}^+ = \Sigma_{\tilde{x},k}^- - L_k \Sigma_{\tilde{y},k} L_k^T$

When the dynamics of the system being modeled is linear, i.e., the functions f and g are linear, the above scheme called KF, and it is the exact minimum mean-square-error state estimator. If the system dynamics is nonlinear, other variants of KF are used. The EKF linearizes the model at each time point, and it performs well when the system nonlinearities are not high. The SPKF (or unscented KF) linearizes the model statistically at each point in time, and it tends to give reasonable estimates even if nonlinearities are high.

In the first phase of purposed SOC estimation method, the parameters a, b, R_0, R, C and the $OCV[k]$ values are estimated by (10)-(16). In the next phase, two types of KF (linear and nonlinear) are purposed depending on the influence of hysteresis effect. If the hysteresis effect is neglected, we can use the following simple linear model window-wise to estimate SOC:

$$SOC[k+1] = SOC[k] + \frac{T\eta}{Q} I[k] + w[k], \quad (18a)$$

$$OCV[k] = aSOC[k] + b + v[k], \quad (18b)$$

where $w[k]$ and $v[k]$ are process and sensor noises with Gaussian distributions. Let us denote this combined estimation scheme (10)-(16) and (18a)-(18b) by ES-KF.

If we are to consider hysteresis effect significantly, the following hysteresis model can be used:

$$OCV = f(SOC) + M_0 s[k] + Mh[k], \quad (19)$$

where $f(SOC)$ denotes the average of main charge curve and discharge curve. In (19), $Mh[k]$ measures the part of hysteresis voltage that changes with SOC and $h[k]$ follows the differential equation:

$$h[k+1] = \begin{cases} e^{-\gamma I[k]T/Q} h[k] + 1 - e^{-\gamma I[k]T/Q}, \text{ if } I[k] \geq 0, \\ e^{\gamma I[k]T/Q} h[k] + e^{\gamma I[k]T/Q} - 1, \text{ if } I[k] < 0, \end{cases} \quad (20)$$

where γ is the hysteresis growth parameter. The voltage $M_0 s[k]$ models the instantaneous hysteresis that measures the change of voltage when current changes the direction suddenly and $s[k]$ is computed by

$$s[k] = \begin{cases} \text{sign}(I[k]), \text{ if } |I[k]| > 0, \\ s[k-1], \text{ otherwise.} \end{cases} \quad (21)$$

The hysteresis modeling (19) is introduced in [13] as a part of enhanced self-correcting model (ESC). The hysteresis effect is very complicated process and there is a certain difficulty for modeling it, we refer to [13] and [17] for the detailed discussions. The parameters M_0, M and γ should be estimated offline for measured values of $OCV - f(SOC)$.

Therefore, the dynamic state-space model of a battery is written as

$$SOC[k+1] = SOC[k] + \frac{T\eta}{Q} I[k] + w[k] \quad , \quad (22a)$$

$$h[k+1] = e^{-\gamma I[k]T/Q} h[k] + \text{sign}(I[k])(1 - \quad e^{-\gamma I[k]T/Q}), \quad (22b)$$

$$OCV[k] = f(SOC[k]) + M_0 s[k] + Mh[k] \quad + v[k]. \quad (22c)$$

The equations (22a) and (22b) are the state equations and (22c) is the output equation for KF algorithm. Note that $V_{RC}[k]$ is not included as one of battery states compared to the original model introduced in [13], since it is determined already from $OCV[k_0]$ window-wise. Similarly with ES-KF, let us denote this co-estimation scheme (10)-(16) and (22a)-(22c) by ES-EKF and ES-SPKF depending on the type of Kalman filter used. The Fig.2 shows the purposed SOC estimation scheme as a flow diagram.

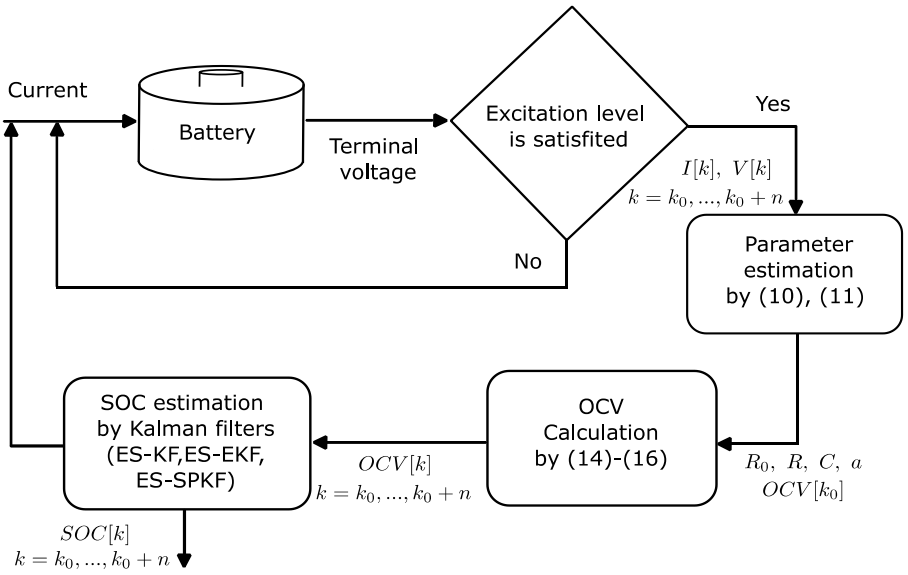

Figure 2. The purposed SOC coestimation algorithm by KFs.

3. RESULTS AND DISCUSSION

In this section, we present the numerical tests to validate our method for three different datasets and discuss the results.

3.1. Test with NMC532/Graphite pouch cell

This section presents the test results for NMC532/Graphite pouch cell. A pouch cell consists of a graphite anode, and NMC532 ($LiNi0.5Mn0.3Co0.2O2$) cathode, where each 21 and 20 two-side coated anode and cathodes are stacked as zig-zag stacking method. This stacked anodes and cathodes are wrapped by Al pouch film with liquid electrolyte. The cell operating voltage range is 3.0 - 4.25V and the maximum continuous charge/discharge current is 0.7C.

A

B

Figure 3. Test bench(a) The NMC532/Graphite pouch cell and the incubator (right) for keeping the cell under 25°C (b) The WBCS-3000s cycler(left) for galvanostatic cell test and the cell test monitoring computer system.

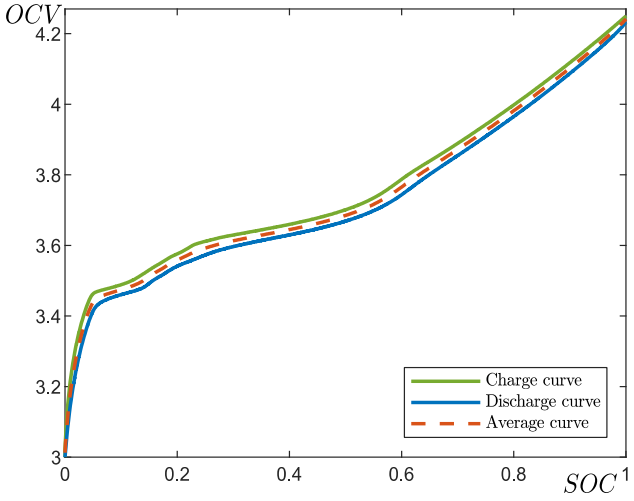

Figure 4. SOC-OCV relation at $T = 25°C$.

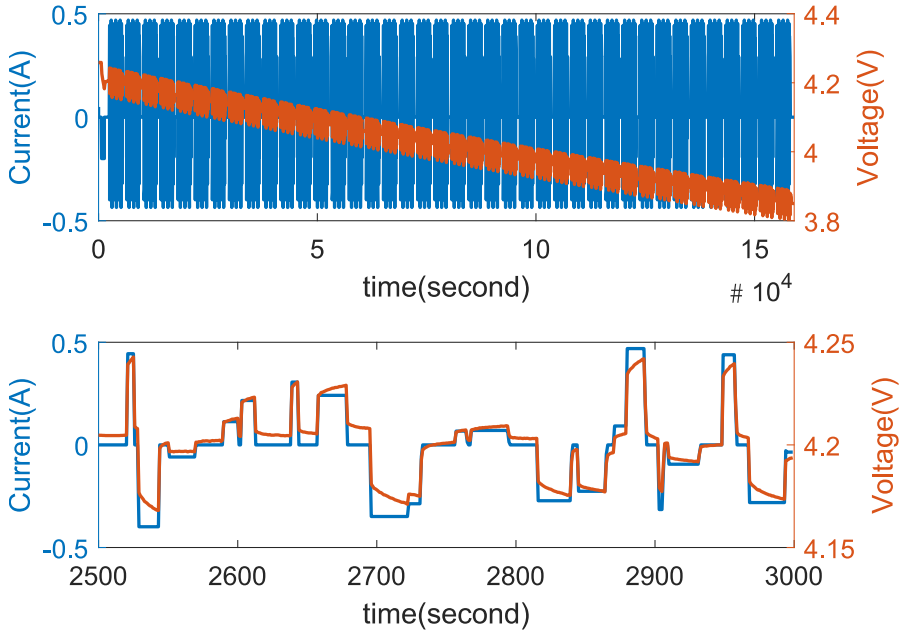

Figure 5. Current and voltage (Lower graph is magnified one of the former).

Model name of charge and discharge cycler is WBCS 3000s . The control voltage range is $\pm 5V$ and the maximum current is $1A$ per each channel. The test equipments are shown in Fig.3ab. The charge and discharge curves (Fig.4) are obtained by $C/30$ current test. All the battery tests are conducted in the battery research and test laboratory at Gwangju Institute of Science and Technology (GIST). For dynamic tests Fig.5, we exercised the dynamic current profile 40 times starting from the initial SOC value of 1, and the last SOC value is 0.68. This dynamic current profile differs from the UDDS profile considered in [14, 45]. As we see from Fig.5, it comprises short constant current intervals.

The estimated hysteresis parameters $\widehat{M_0}, \widehat{M}$ and $\hat{\gamma}$ for different SOC values are tabulated in Table.1 and M and M_0 linearly estimated parameters for $\gamma = 6.5411$, which is the average value of $\hat{\gamma}$. Instantaneous hysteresis parameter M_0 is estimated with very small negative values. This tells us instantaneous hysteresis has some small reverse effect for constant current profile, if we compare it to the latter section, where the considered UDDS current profile has many sudden jumps. Consequently, it says instantaneous hysteresis could have different characteristics depending on the current history. Its effect on overall SOC estimation is very little and some comparisons were made in [45]. In Fig.6, the extracted parameters R_0, R, C, a, b and window sizes with excitation level 53 are graphed against the number of window. The excitation level is a crucial parameter that decides the time window and it should be tuned carefully. Higher value generates longer time windows and smaller value (therefore, shorter time window length) may cause numerical stability. In this experiment, the average length of time windows was 630. The variability of R_0 and R is clearly shown, while C takes the average value of 434 most of the times.

Table 1. Offline estimation of M_0, M and γ.

SOC	M	M_0	$\widehat{M}$	$\widehat{M_0}$	$\hat{\gamma}$
0.964	0.026	-2.5e-05	0.032	-0.00015	14.7
0.956	0.034	-3.3e-05	0.039	-0.00014	12.0
0.949	0.042	-4.0e-05	0.045	-0.00015	11.9
0.942	0.049	-6.9e-05	0.051	-0.00015	10.1
0.935	0.057	-5.9e-05	0.058	-0.00012	9.1
0.928	0.063	-9.4e-05	0.064	-0.00014	8.1
0.921	0.071	-0.00014	0.072	-0.00017	7.4
0.914	0.074	-0.00016	0.074	-0.00019	7.3
0.907	0.079	-0.00014	0.079	-0.00017	7.1
0.899	0.087	-0.00015	0.087	-0.00016	6.7
0.892	0.092	-0.00020	0.092	-0.00019	6.2
0.885	0.099	-0.00022	0.099	-0.00019	5.8
0.878	0.102	-0.00023	0.102	-0.00020	5.8
0.871	0.107	-0.00020	0.107	-0.00017	5.9
0.864	0.115	-0.00023	0.115	-0.00018	5.6
0.857	0.121	-0.00028	0.121	-0.00020	5.0
0.850	0.129	-0.00029	0.129	-0.00021	4.9
0.842	0.133	-0.00031	0.134	-0.00023	5.1
0.835	0.140	-0.00032	0.140	-0.00023	4.9
0.828	0.148	-0.00032	0.148	-0.00022	4.8
0.821	0.157	-0.00038	0.157	-0.00025	4.4
0.814	0.164	-0.00041	0.165	-0.00026	4.3
0.807	0.166	-0.00043	0.167	-0.00029	4.5
0.800	0.170	-0.00043	0.171	-0.00028	4.4
0.793	0.177	-0.00043	0.177	-0.00030	4.7
0.786	0.181	-0.00049	0.182	-0.00032	4.3
0.779	0.187	-0.00051	0.188	-0.00033	4.2

SOC	M	M_0	$\widehat{M}$	$\widehat{M_0}$	$\hat{\gamma}$
0.771	0.190	-0.00048	0.190	-0.00033	4.6
0.764	0.194	-0.00049	0.195	-0.00035	4.8
0.757	0.202	-0.00051	0.202	-0.00037	4.8
0.750	0.208	-0.00056	0.209	-0.00039	4.5
0.743	0.214	-0.00055	0.215	-0.00037	4.5
0.736	0.216	-0.00055	0.217	-0.00040	4.9
0.729	0.221	-0.00054	0.222	-0.00041	5.0
0.721	0.228	-0.00053	0.228	-0.00041	5.2
0.714	0.234	-0.00060	0.235	-0.00045	4.8
0.707	0.241	-0.00059	0.242	-0.00044	5.0
0.700	0.245	-0.00057	0.246	-0.00045	5.3

In Fig.7, the estimated OCV (purple) and the terminal voltage V(light blue) are graphed for the same time interval as in Fig.5. Compared the magnitudes of OCV and V, it is seen that the dynamics of electrical circuit model explains much part of the terminal voltage. Ideally, if SOC-OCV relation is just one curve (that is there is no hysteresis effect), one would expect the estimated OCV is smooth piece-wise lines that coincides with SOC-OCV curve. However, as seen in Fig.7, the identified OCV values are not exactly piece-wise lines because of the hysteresis effect. Based on the estimated hysteresis parameters in Table.1, we see this remaining voltage difference is modeled with enough accuracy by the hysteresis model (19). Another important observation is the average SOC-OCV curve can be approximated by the fitted curve of OCV values with some offset. We show the average SOC-OCV curve can be extracted from the driving cycle data in section 3.3.

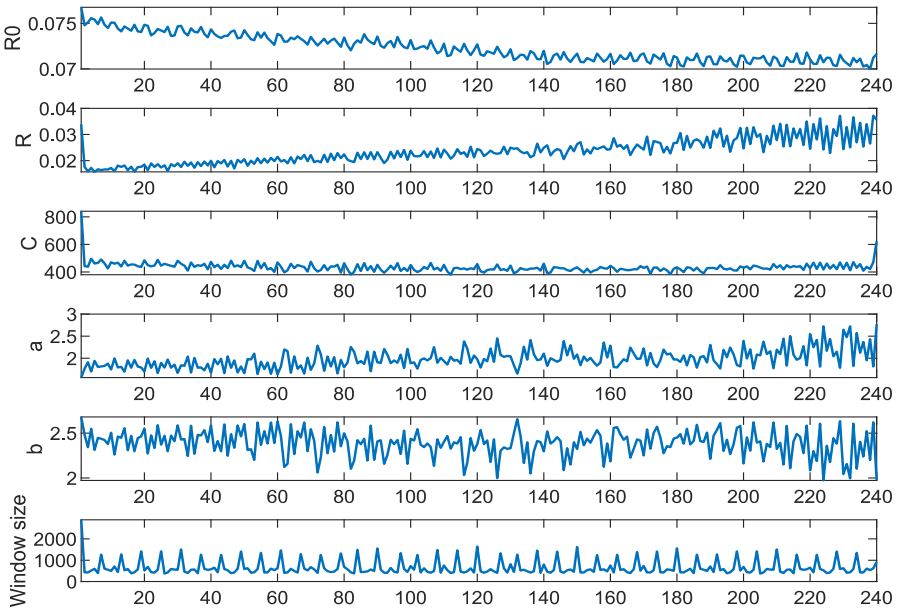

Figure 6. Estimated parameters and time window sizes with excitation level 53 (x axis is for the number of time window).

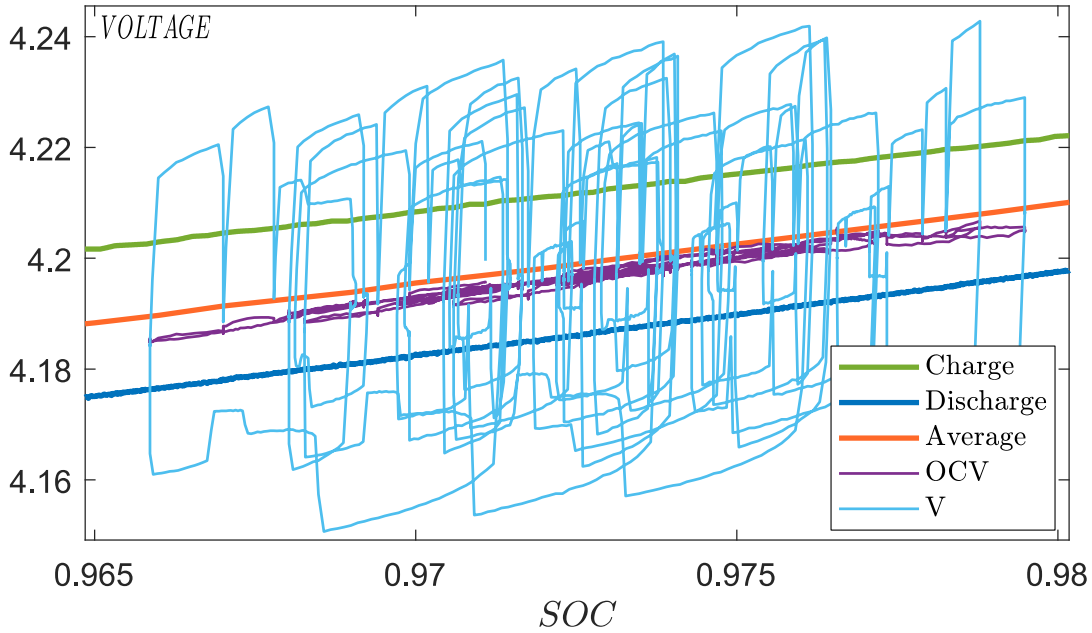

Figure 7. The terminal voltage and the estimated OCV.

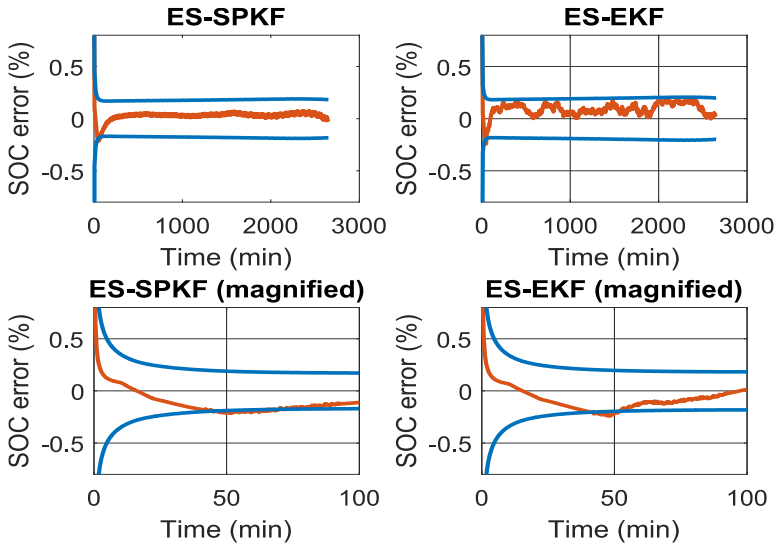

Figure 8. Error bounds of ES-SPKF and ES-EKF estimations.

Table 2. $\boldsymbol{SOC}$ estimation errors (in percents).

Methods	ES-KF	ES-EKF	ES-SPKF
RMS	0.0890%	0.1091%	0.0517%
MAE	0.0785%	0.0967%	0.0388%
MAX	3.3%	2.970%	2.9718%
EOB	0.0046%	0.4112%	0.9%

Finally, the result of SOC estimation is presented in Table.2, where the root mean square error (RMS), mean absolute error (MAE), maximum absolute error (MAX) and the error outside 3-sigma limit (EOB) are tabulated. The noise variances for KF-based estimations are chosen to be $\Sigma_w = 2e-3$ and $\Sigma_v = 2e-3$ by trail and error test. The error bounds for ES-EKF and ES-SPKF are presented in Fig. 8. Both ES-EKF and ES-SPKF algorithms perform almost equally in this experiment. Starting from wrong initial SOC value 0.98, the 3-sigma bound enters the interval $[-0.5\%, 0.5\%]$ in first 5 minutes and the error never leaves the bound $[-0.2\%, 0.2\%]$. Because of the nonlinearity involved, the error of ES-EKF fluctuates, while ES-SPKF shows more stable trend. The error for ES-KF is comparable to that of two others. Considering the less computational effort and the estimation accuracy of ES-KF, the ES-KF algorithm can be a reasonable candidate in the pool of SOC estimation algorithms for this experiment. However, we will see this may not be the case for different battery experiments in the next sections.

3.2. Test with lithium-ion "E2" cell

In this section, we compared the performances of the proposed methods ES-KF, ES-EKF and ES-SPKF with that of EKF and SPKF reported in [13] for lithium-ion "E2" cell data and for two ambient temperatures $T = 5°C$ and $T = 25°C$. The battery's current and terminal voltage is displayed in Fig.9. This data is obtained by repeatedly exercising the "urban dynamometer drive schedule" (UDDS) profile. There are around 720 seconds of rest time after each UDDS profile exercise. Fig.10 shows the charge and discharge curves at the temperatures $T = 5°C$ and $T = 25°C$.

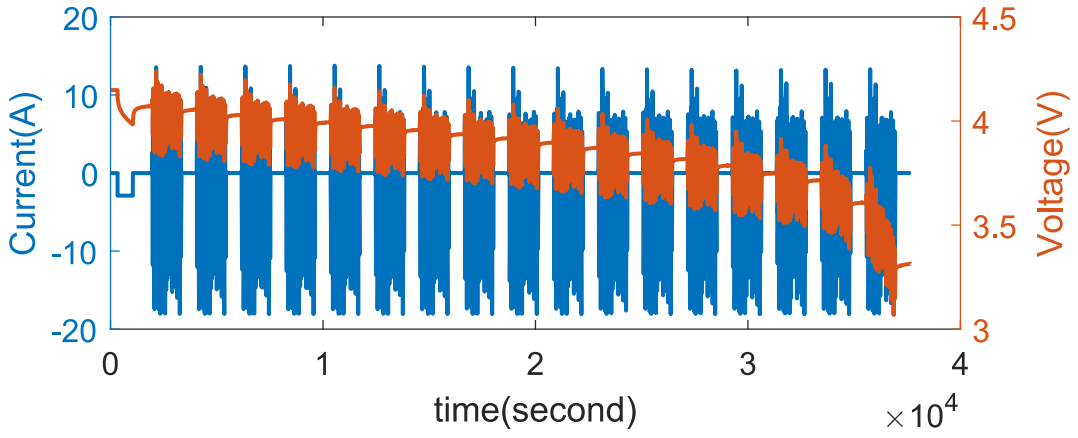

Figure 9. Current and voltage of dynamic test data of the UDDS pattern $(T = 25°C)$

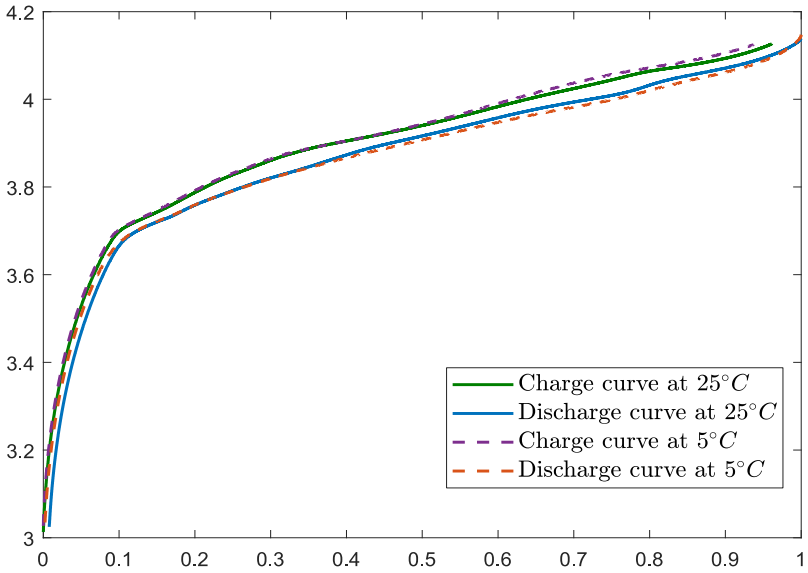

Figure 10. SOC-OCV relation at $T = 5°C$ and $T = 25°C$

Table 4 and 5 show the values of M, M_0 estimated linearly for $\gamma_{25} = 39.6, \gamma_5 = 64.4$, which are taken as the averages of estimated values $\hat{\gamma}$ for each temperature. We observed that for the case $T = 25°C$ the instantaneous hysteresis parameter M_0 is estimated significantly compared with that reported in [45]. This is because the rectangle rule for integral used in (9) captures the instantaneous hysteresis more efficiently, whereas the trapezoidal rule for integral was used instead in [45]. Another effect observed in Table 5 is hysteresis level for $T = 5°C$ is higher than for $T = 25°C$, which is expected, since the battery dynamics is more severe in cooler temperatures. Fig.11 shows the estimated parameters and time window sizes. The excitation level 790 was found suitable for this experiment. The higher excitation level is due to the rest time of 720 seconds in the test data. Note that the excitation level can be reduced significantly by excluding the interval of rest time from the least square estimation, since the hysteresis voltage changes in an adverse way during it .

The values of R_0, R and C shown in Table 3 and the noise covariances $\Sigma_w = 0.2$ and $\Sigma_v = 0.2$ are the parameters values used in the original ESC model for SPKF and EKF in [13]. The performances of the methods ES-KF, ES-EKF, ES-SPKF, EKF and SPKF are compared in Table 6 and Fig. 12, 13. All the methods use the same noise covariances $\Sigma_w = 0.2$ and $\Sigma_v = 0.2$.

Table 3. The parameters reported in [13].

	$R0$	R	C	M	M_0
$T = 25°C$	0.0112	0.0025	958.4886	0.0443	0.0025
$T = 5°C$	0.0313	0.0071	254.9203	0.0805	0

Table 4. Offline estimation of M_0, M and γ for $T = 25^{\circ}C$.

SOC	M	M_0	$\widehat{M}$	$\widehat{M_0}$	$\hat{\gamma}$
0.887	0.040	0.0034	0.042	0.0042	125.5
0.840	0.052	0.0021	0.052	0.0022	70.2
0.793	0.047	0.0022	0.047	0.0021	59.1
0.746	0.046	0.0021	0.045	0.0022	74.5
0.699	0.049	0.0021	0.049	0.0022	70.2
0.652	0.053	0.0023	0.054	0.0022	57.8
0.604	0.057	0.0024	0.057	0.0023	57.0
0.557	0.059	0.0024	0.059	0.0023	57.0
0.510	0.062	0.0026	0.062	0.0024	57.0
0.463	0.068	0.0025	0.069	0.0023	57.0
0.416	0.077	0.0027	0.077	0.0025	57.0
0.369	0.091	0.0032	0.091	0.0029	57.0
0.322	0.100	0.0035	0.100	0.0032	57.0
0.275	0.096	0.0036	0.097	0.0033	57.0
0.228	0.090	0.0035	0.090	0.0032	57.0
0.181	0.078	0.0028	0.078	0.0026	57.0
0.134	0.115	0.0022	0.115	0.0026	74.5
0.087	0.228	0.0053	0.229	0.0046	57.0

Table 5. Offline estimation of M_0, M and γ for $T = 5^{\circ}C$.

SOC	M	M_0	$\widehat{M}$	$\widehat{M_0}$	$\hat{\gamma}$
0.887	0.009	-0.0007	0.013	0.00062	123.5
0.836	0.031	0.0007	0.029	0.00102	66.3
0.786	0.031	0.0008	0.030	0.00132	51.3
0.735	0.029	0.0005	0.028	0.00097	51.3
0.684	0.033	0.0006	0.032	0.00099	47.0
0.633	0.037	0.0009	0.036	0.00111	43.4
0.582	0.038	0.0010	0.038	0.00115	42.7
0.532	0.041	0.0011	0.041	0.00122	42.4
0.481	0.046	0.0013	0.046	0.00132	40.4
0.430	0.061	0.0021	0.062	0.00123	30.4
0.379	0.088	0.0040	0.094	0.00078	16.7
0.328	0.100	0.0052	0.109	0.00065	11.4
0.278	0.091	0.0046	0.098	0.00063	12.5
0.227	0.077	0.0038	0.082	0.00066	13.9
0.176	0.054	0.0023	0.057	0.00059	18.3
0.125	0.060	0.0007	0.059	0.00093	42.1
0.074	0.102	0.0034	0.107	0.00038	19.7

Because of the hysteresis voltage, the initial value $SOC[k_0]$ and b determined by (13) have large error. This causes the uncertainty in the measurement equation grow so big that ES-KF suffers from large error bound and very unstable SOC estimation as depicted in Fig.13. This result is in contrast with the previous section, where the maximum charge/discharge current is 0.5A.

The methods EKF, SPKF, ES-EKF and ES-SPKF, which model the hysteresis voltage, yield comparable results with each other. Among them, the methods ES-EKF and ES-SPKF perform better than EKF and SPKF [13] and they are improving the results in [45] where the least square SOC estimator was used.

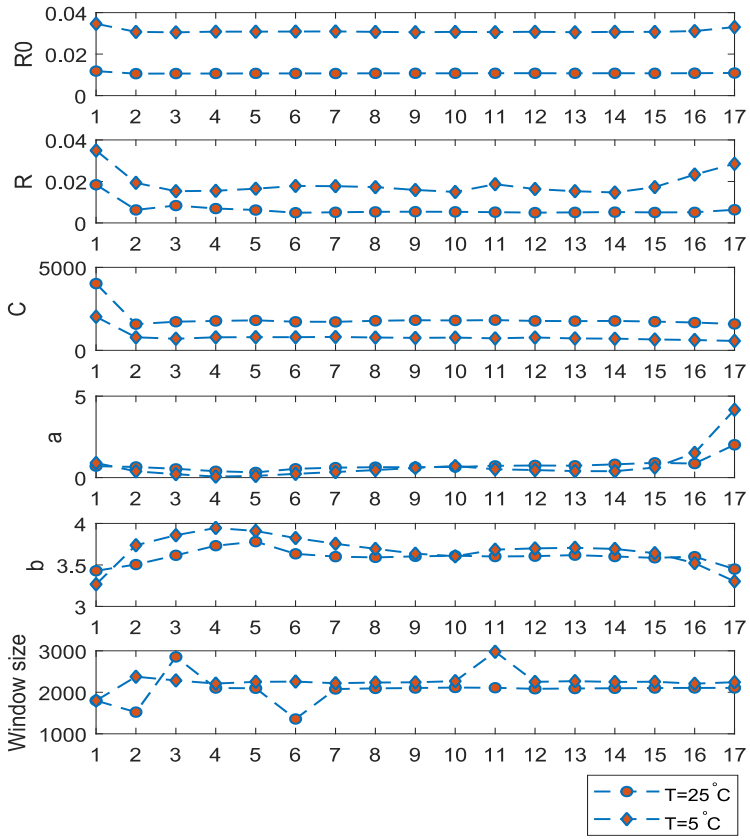

Figure 11. Estimated parameters and time window sizes for $T = 25°C$ and $T = 5°C$ with excitation level 790 (x axis is for the number of time window).

Table 6. RMS errors (in percents).

Methods	$T = 25°C$	$T = 5°C$
ES-KF	2.6363%	8.6335%
EOB	4.9495%	36.9960%
EKF	0.5104%	1.5252%
EOB	2.0286%	35.9171%
ES-EKF	0.1580%	0.5696%
EOB	0%	0%
SPKF	0.5341%	0.8368%
EOB	3.6723%	10.5274%
ES-SPKF	0.1569%	0.2650%
EOB	0%	0.2783%

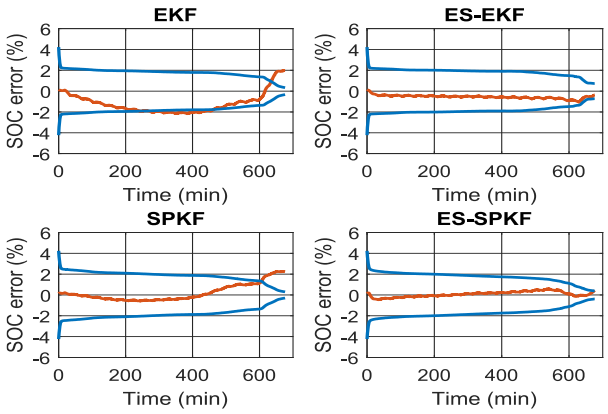

Figure 12. Error bounds for $T = 5°C$

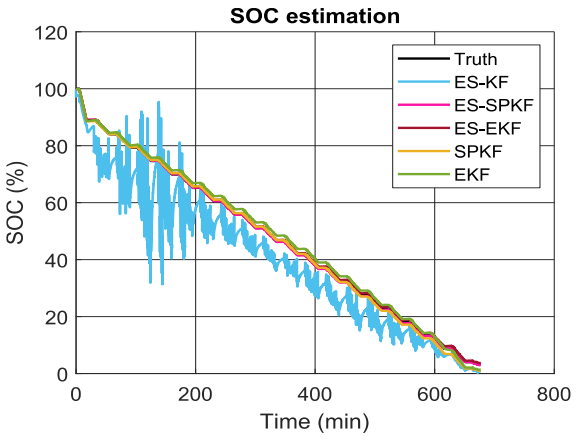

Figure 13. SOC estimation for $T = 5°C$

The method ES-SPKF outperforms all the others because of it's efficient handling of nonlinearity. The improvement of ES-EKF and ES-SPKF can be explained by two ideas proposed in this work. First, the nonlinearity in battery dynamics localized efficiently and the parameters are extracted online with dependence on the SOC as in Fig.14. Second, the initial value $OCV[k_0]$ is estimated along with other parameters and it enables us to calculate all $OCV[k]$. This process lets us to use fewer state equations (22a) and (22b) in KF algorithm

3.3. Test with 18650 PF Battery

In this section, the ES-EKF and ES-SPKF algorithms tested for 18650PF Li-ion battery dataset, which is publicly available at [49] and used by the deep-learning based SOC estimation methods reported in [50, 7, 8]. The 18650PF Li-ion battery has $LiNiCoAlO_2$ chemistry, and $2.9Ah$ nominal capacity. The dataset includes four basic dynamic driving tests: UDDS, HWFET, LA92 and US06, and random mixes of them: Cycle-1, Cycle-2, Cycle-3, Cycle-4 and NN. The original data which has 10Hz sample rate converted to the data with 1Hz sample rate, and the current and voltage for Cycle-3 pattern was shown

in Fig. 14. Since the data set does not contain the SOC-OCV curve (obtainable by C/30 test), the first task is the acquisition of SOC-OCV relation based on the available driving cycle data.

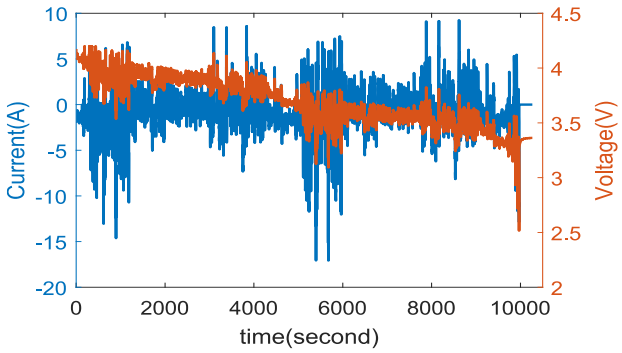

Figure 14. Current and voltage of dynamic test data of the Cycle-3 pattern for $T = 25^{\circ}C$

In order to do so, we obtain OCV values for each test by executing (10)-(16) algorithm. Fig.15 shows the estimated OCV values for each driving test cases and the average SOC-OCV curve, which is fitted by 7-th order polynomial with coefficients

$$p = [-32.4,\ 122.3, -181.7,\ 131.5, -44.5,\ 3.9,\ 1.8,\ 3.1].$$

Compared to the previous experiments, there are many driving cycle patterns in this dataset. If we repeat the offline estimations of M, M_0, γ with dependence on SOC for each driving cycle, we get slightly different values. We did not see any reasonable SOC dependence for averaged values of them. This suggests that the values of M, M_0, γ must be generalized over entire data. Therefore, we estimated M, M_0, γ for each driving cycle without SOC dependence and averaged them over all driving cycles. The average values are found to be $M = 0.0482$, $M_0 = -4.34e-5, \gamma = 36.3289$ and the experiments show they generalize good enough the hysteresis effect.

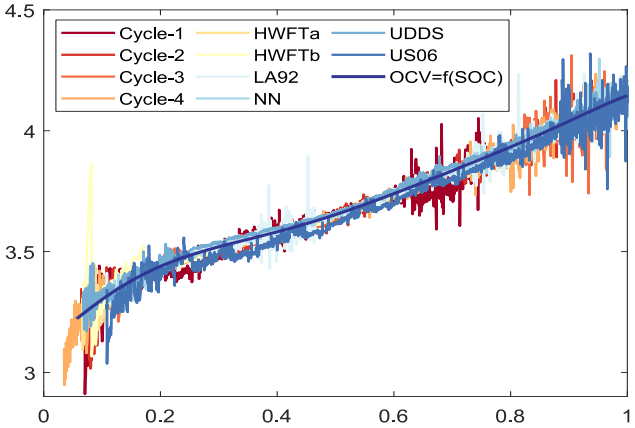

Figure 15. SOC-OCV curve estimated by nonlinear regression.

As an example, Fig. 16 presents the estimated parameters and time window sizes with the excitation level 600 and SOC estimation error and bounds are shown in Fig. 17 for Cycle-3 driving cycle. The sensor noise covariance $\Sigma_w = 0.002$ and the measurement noise covariance $\Sigma_v = 0.2$ are experimentally found.

Table 7 shows the SOC estimation results of two methods ES-SPKF and ES-EKF for the faulty initialization of $SOC_0 = 0.99$. Generally, the estimation errors are in the same order for the mixed driving cycle datasets: Cycle-1, Cycle-3, Cycle-3, Cycle-4, which indicates the SOC-OCV curve and the parameters M, M_0, γ generalized good enough over the entire dataset. The error for US06 pattern takes the highest value. This is because the US06 pattern has much higher current discharge rate and it is more challenging case compared to the others [50].

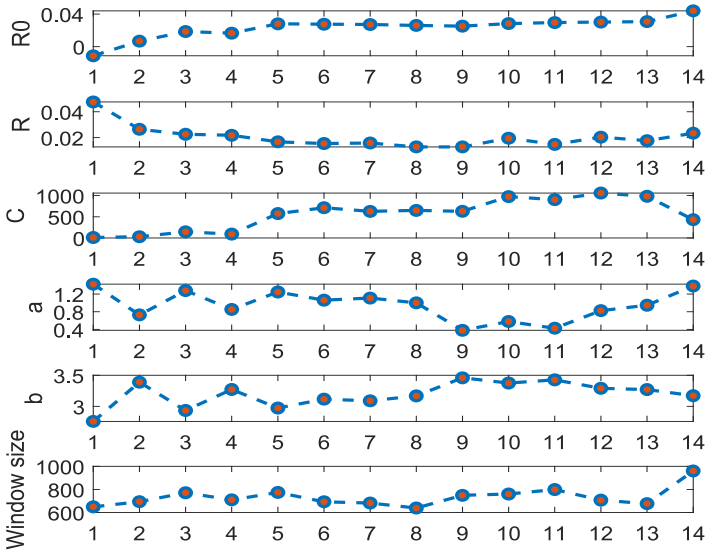

Figure 16. Estimated parameters and time window sizes for Cycle-3 for $T = 25°C$ (x axis is for the number of time window).

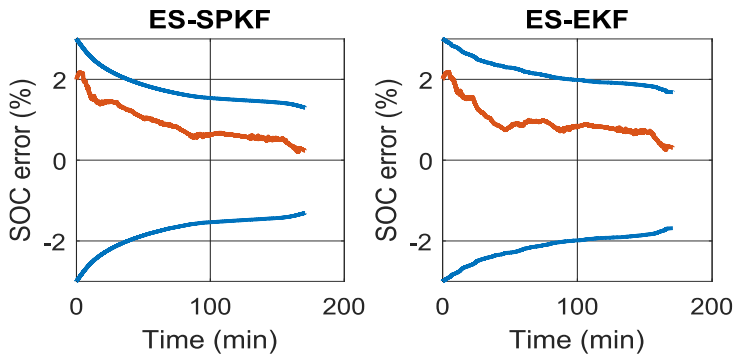

Figure 17. SOC estimation error and error bounds for Cycle-3 and $T = 25°C$ with the faulty initialization of $SOC_0 = 0.8$.

Because of handling uncertainty differently (initial SOC value and, assumed noise levels), it is difficult to directly compare our method and the machine learning based methods [50, 7, 8]. But, we see

the result of our method is in competitive order with the average error values $RMS = 0.5076,\ MAE = 0.4367,\ MAX = 1.0294$ for ES-SPKF.

3.4. Discussion

Based on the results of three different datasets, the ES-KF method is only applicable when the charge/discharge current is in some low level or the polarization of hysteresis voltage is small and negligible. However, ES-EKF and ES-SPKF are the universal approaches to estimate SOC when SOC-OCV curve is extracted with enough accuracy and the hysteresis parameters $M,\ M_0,\ \gamma$ are estimated and generalized well over various driving cycles. More sophisticated method to adjust time window size may be implemented in practice to adapt to various current profiles. One approach is to set conditions on both minimum length of time window and excitation count (12). In general, the purposed KF based SOC coestimation scheme is robust and simple yet. It can yield accurate results when model parameters tuned up and generalized well. In order to implement temperature-dependent version of this method, it is enough to obtain SOC-OCV curves and the parameters $M,\ M_0,\ \gamma$ at a few different temperatures and interpolate the intermediate values, since other parameters are determined online. The SOC-OCV curve can be obtained from dynamic data by our method without the lengthy C/30 experiments. Our method can be extended naturally to estimate battery health ($R_0,\ Q$) by employing joint and dual nonlinear KFs.

4. CONCLUSION

Online parameter identification and KF-based battery SOC estimation technique were proposed for an electrical battery model. Firstly, modeling the SOC-OCV relation locally linear on the fly, we perform a simple linear least square estimation algorithm with variable-length time window and extract battery parameters R_0, R, C, a, b and $OCV[k_0]$. This procedure lets us obtain values of OCV window-wise. In the next phase, ES-KF, ES-EKF and ES-SPKF algorithms are executed to estimate the SOC with fewer state equations. Extensive experimental tests are conducted for the real data obtained in the designated labs. The ES-EKF and ES-SPKF methods with model parameters estimated online perform better than the other methods considered previously and the performances are in competitive manner with machine learning based methods.

ACKNOWLEDGEMENTS
Funding: This work was supported by the National Research Fund with numbers 2017R1E1A1A03070061 and 2020R1I1A3071769.

References

1. K. S. Ng, C.-S. Moo, Y.-P. Chen, and Y.-C. Hsieh, *Appl. Energy*, 86 (2009) 1506

2. F. Codeca, S. M. Savaresi, and V. Manzoni, in Proceedings of the 48h IEEE Conference on Decision and Control (CDC) held jointly with 2009 28th Chinese Control Conference, (2009), 8083.
3. M. Coleman, C. K. Lee, C. Zhu, and W. G. Hurley, *IEEE Trans. Ind. Electron*., 54 (2007) 2550.
4. H. Sheng and J. Xiao, *J. Power Sources*, 281 (2015) 131.
5. F. Yang, W. Li, C. Li, and Q. Miao, *Energy*, 175 (2019) 66.
6. M. S. Hossain Lipu, M. A. Hannan, A. Hussain, M. H. Saad, A. Ayob, and M. N. Uddin, *IEEE Trans. Ind. Appl.*, 55 (2019) 4225.
7. E. Chemali, P. J. Kollmeyer, M. Preindl, R. Ahmed, and A. Emadi, *IEEE Trans. Ind. Electron*., 65 (2018) 6730.
8. A. Bhattacharjee, A. Verma, S. Mishra, and T. K. Saha, *IEEE Trans. Veh. Technol*., 70 (2021) 3123.
9. D. N. T. How, M. A. Hannan, M. S. Hossain Lipu, and P. J. Ker, *IEEE Access*, 7 (2019) 136116.
10. M. Chen and G. A. Rincon-Mora, *IEEE Trans. Energy Convers*., 21 (2006) 504.
11. R. A. Jackey, M. Saginaw, P. Sanghvi, J. Gazzarri, T. Huria, and M. Ceraolo, in SAE Technical Paper, *SAE International*, 04 (2013) 1547.
12. R. A. Jackey, G. L. Plett, and M. J. Klein, in SAE Technical Paper, *SAE International*, 04 (2009) 1381.
13. G. Plett, Battery Management Systems, Volume I: Battery Modeling, Artech House Power Engineering series, Artech House, 2015.
14. G. Plett, Battery Management Systems, Volume II: Equivalent-Circuit models, Artech House Power Engineering series, Artech House, 2016.
15. G. L. Plett, *J. Power Sources*, 134 (2004) 252.
16. Z. Chen, Y. Fu, and C. C. Mi, *IEEE Trans. Veh. Technol*., 62 (2013)1020.
17. J. L. Z. Cheng, L. Wang and J. Lv, *Tehnicki vjesnik*, 23 (2016) 695.
18. Z. Zeng, J. Tian, D. Li, and Y. Tian, *Energies*, 11 (2018) 59.
19. E. Locorotondo, G. Lutzemberger, and L. *Pugi*, *Proc. Inst. Mech. Eng., Part I: J. Syst. Control Eng.*, 235 (2021) 1272.
20. C. Jiang, S. Wang, B. Wu, C. Fernandez, X. Xiong, and J. Coffie-Ken, *Energy*, 219 (2021) 119603.
21. W. Cao, S.-L. Wang, C. Fernandez, C.-Y. Zou, C.-M. Yu, and X.-X. Li, *Energy Sci. Eng*., 7 (2019) 1544.
22. Y. Zhang, S. Wang, W. Xu, C. Fernandez, and Y. Fan, *Int. J. Electrochem. Sci*., 16 (2021) 210624.
23. Z. Zhang, L. Jiang, L. Zhang, and C. Huang, *J. Energy Storage*, 37 (2021) 102457.
24. H. He, R. Xiong, X. Zhang, F. Sun, and J. Fan, *IEEE Trans. Veh. Technol*., 60 (2011) 1461.
25. X. Guo, L. Kang, Y. Yao, Z. Huang, and W. Li, *Energies*, 9 (2016) 100.
26. X. Lin, Y. Tang, J. Ren, and Y. Wei, *J. Energy Storage*, 41 (2021) 102840.
27. D. Jiani, W. Youyi, and W. Changyun, in 2013 10th IEEE International Conference on Control and Automation (ICCA), (2013) 580.
28. K. Zhang, J. Ma, X. Zhao, D. Zhang, and Y. He, *IEEE Access*, 7 (2019) 166657.
29. Q. Ouyang, J. Chen, F. Wang, and H. Su, 19th IFAC World Congress , IFAC Proceedings Volumes, 47 (2014) 2794.
30. Y. Ma, B. Li, G. Li, J. Zhang, and H. Chen, *IEEE/CAA J. Autom. Sin*., 4 (2017) 195.
31. H. Rahimi-Eichi, F. Baronti, and M. Chow, *IEEE Trans. Ind. Electron*., 61 (2014) 2053.
32. J. Xu, C. C. Mi, B. Cao, J. Deng, Z. Chen, and S. Li, *IEEE Trans. Veh. Technol*., 63 (2014) 1614.
33. I.-S. Kim, *IEEE Trans. Power Electron*., 23 (2008) 2027.
34. F. Zhang, G. Liu, and L. Fang, in 2008 7th World Congress on Intelligent Control and Automation, (2008) 989.
35. A. Nath, R. Gupta, R. Mehta, S. S. Bahga, A. Gupta, and S. Bhasin, *IEEE Trans. Veh. Technol*., 69 (2020) 14701.
36. B. Ning, B. Cao, B. Wang, and Z. Zou, *Energy*, 153 (2018) 732.

37. W. Waag, C. Fleischer, and D. U. Sauer, *J. Power Sources*, 258 (2014) 321.
38. C. Zhang, K. Li, S. Mcloone, and Z. Yang, in 2014 European Control Conference (ECC), (2014) 2673.
39. Y. Wang, H. Fang, L. Zhou, and T. Wada, *IEEE Control Syst. Mag.*, 37 (2017) 73.
40. A.M.S.M.H.S.Attanayaka, J.P.Karunadasa, and K.T.M.U.Hemapala, AIMS Energy, 7 (2019) 186.
41. H. Rahimi-Eichi, F. Baronti, and M. . Chow, in 2012 IEEE International Symposium on Industrial Electronics, (2012) 1336.
42. H. Rahimi-Eichi and M. Chow, in 2013 IEEE Transportation Electrification Conference and Expo (ITEC), (2013) 1.
43. H. Rahimi-Eichi and M. Chow, in IECON 2012 - 38th Annual Conference on IEEE Industrial Electronics Society, (2012) 4012.
44. R. A. El-Sehiemy, M. Hamida, and T. Mesbahi, *Int. J. Hydrogen Energy*, 45 (2020) 8833.
45. M. Kwak, B. Lkhagvasuren, J. Park, and J. You, *IEEE Trans. Ind. Electron.*, 67 (2020) 9758.
46. H. Wang, Y. Zheng, and Y. Yu, *Mathematics*, 9 (2021).
47. Y. Xu, M. Hu, A. Zhou, Y. Li, S. Li, C. Fu, and C. Gong, *Appl. Math. Modell.*, 77 (2020) 1255.
48. J. Jiang and Y. Zhang, *Int. J. Adapt. Control Signal Process.*, 18 (2004) 505.
49. P. Kollmeyer, 18650 PF li-ion battery data. (2018).
50. C. Vidal, P. Kollmeyer, M. Naguib, P. Malysz, O. Gross, and A. Emadi, Robust xEV Battery State-of-Charge Estimator Design Using a Feedforward Deep Neural Network , *Technical paper*, (2020) 1181.